Int. J. Solids Structures Vol. 22, No. 4, pp. 373–386, 1986
Printed in Great Britain.

0020-7683/86 $3.00 + .00
Pergamon Journals Ltd.

MODELLING OF THE COUPLED EFFECT OF PLASTIC DAMAGE AND CREEP DAMAGE IN NIMONIC 80A

S. MURAKAMI†
Department of Mechanical Engineering, Nagoya University, Chikusa-ku, Nagoya 464, Japan

Y. SANOMURA
Department of Mechanical and Electrical Engineering, Tokuyama Technical College, Kume, Tokuyama 745, Japan

and

M. HATTORI
Department of Energy Engineering, Toyohashi University of Technology, Tempaku-cho, Toyohashi 440, Japan

(*Received* 29 *November* 1984; *in revised form* 12 *April* 1985)

Abstract—The title problem was discussed from a viewpoint of continuum damage mechanics. By assuming that both the plastic and the creep damages are governed by the formation and the growth of the grain boundary cavities, the states of plastic and creep damages caused by these cavities were first represented in terms of a symmetric second-rank damage tensor. The interaction between these two kinds of damage was formulated by establishing the evolution and the constitutive equation of the damaged materials on the basis of the experimental observations on microscopic mechanisms of these damages and their mechanical effects reported so far. Finally, the effects of material damage induced by prior plastic strain in tension, compression and torsion at room temperature on the subsequent creep and creep rupture process of Nimonic 80A at 750°C were analysed by these equations, and the validity and the limitations of the proposed theory were discussed by comparing the numerical results with the corresponding experimental ones. It was observed that the proposed theory not only described well the significant reduction of creep strength and creep rupture time brought about by the preceding plastic deformation at room temperature, but it also represented adequately the anisotropic features of plastic and creep damages.

1. INTRODUCTION

Elastic–plastic deformations in polycrystalline metals and alloys often induce internal damage of materials[1–5]. This internal damage usually occurs by the nucleation and growth of various microscopic cracks and cavities produced by the deformation. Such elastic–plastic damage, therefore, not only gives significant influence on the mechanical properties of materials but also causes material deterioration, such as reduction of ductility, rigidity, strength, remaining life time, etc. The problems of elastic–plastic damage, therefore, have been the objectives of a number of works from metallurgical and continuum mechanics points of view[1–5]. Particularly, the effects of elastic–plastic damage at room temperature on the subsequent creep behaviour of the materials have been discussed in a series of the experimental and the theoretical papers of Dyson and Rodgers[6], Dyson, Loveday and Rodgers[7] and Hayhurst, Trampczynski and Leckie[8].

The elastic–plastic damage not only has salient anisotropy just like the creep damage but also has much more complicated microscopic mechanisms than the creep damage; these mechanisms depend strongly on the type of stress variation. Thus, unlike the case of creep damage, systematic modelling of the elastic–plastic damage from a continuum mechanics point of view[9–12] is rather scarce, and no general anisotropic theories capable of describing the coupled effects of the elastic–plastic and the creep damages have been developed so far.

The present paper is concerned with the formulation of the coupled phenomena of plastic and creep damages in polycrystalline metals by describing the anisotropic

† Author to whom correspondence should be sent.

damage states in terms of a damage tensor of rank two[13–16]. The evolution and the constitutive equations are developed by incorporating the experimental observations on the mechanisms of these damages and their mechanical effects reported so far. The validity and the limitations of the proposed theory are discussed by analysing the creep damage process of Nimonic 80A subjected to prior plastic strain of tension and torsion, and by comparing these results with the corresponding experimental ones. This problem was analysed also by Hayhurst *et al.*[8] in the framework of isotropic damage theory.

2. FORMULATION OF COUPLED PHENOMENA OF PLASTIC DAMAGE AND CREEP DAMAGE

The elastic–plastic damage at the temperature range of significant slip or grain boundary sliding mostly develops by the formation of various grain boundary cavities[17–21]. The grain boundary cavities, in turn, are induced by the intersection of slip with a grain boundary or with precipitates on a grain boundary, or by the blocking of grain boundary sliding due to triple points, ledges or impurity particles on the grain boundaries, together with the resulting stress concentration[7, 18, 21]. Therefore, the orientation and the arrangement of these cavities depend largely on the direction of the applied stress. Dyson, Loveday and Rodgers[7], for example, observed microstructural changes of Nimonic 80A caused by plastic prestrains of tension, compression and torsion by means of a high-voltage electron microscope, and they found the formation of profuse submicrometer cavities, mainly on grain boundaries parallel to the maximum principal stress direction.

The cavities as a result of creep damage, on the other hand, are induced by the stress concentration due to grain boundary sliding at various irregularities on the boundaries such as grain corners, triple points, ledges, steps and impurity particles[22, 23]. These cavities develop most markedly on grain boundaries perpendicular to the maximum principal stress direction and show salient anisotropy[17, 22–25]. In some cases, especially for relatively high stresses, creep cavities are observed also on grain boundaries parallel to the direction of maximum shearing stress[34].

The elastic–plastic damage mentioned above has been discussed in the framework of continuum damage mechanics by several authors. Broberg[26] and Hult[27], for example, extended the creep damage theory of Kachanov–Rabotnov[28] to include the time-independent elastic–plastic damage under uniaxial states of stress. Lemaitre and Chaboche[2] and Lemaitre[3], on the other hand, developed another theory of one-dimensional elastic–plastic damage by defining a damage variable in terms of the change of elastic modulus of the material and by postulating a threshold stress σ_s for the initiation of time-independent damage. If we assume the isotropy of the damage states, these theories may be readily generalized to multiaxial states of stress. However, formulation of a more elaborate anisotropic damage theory requires us to describe the damage states by means of a more proper damage variable. In the following, we will develop an anisotropic plastic damage model by modifying the creep damage theory of Murakami and Ohno[14], which describes the anisotropic damage states in terms of a second-rank symmetric *damage tensor* $\boldsymbol{\Omega}$. Though the second-rank tensor $\boldsymbol{\Omega}$ cannot describe the damage states with more complicated symmetry than orthotropy[12], it facilitates the feasible modelling of anisotropic damage because of its mathematical simplicity.

If we restrict our attention to plastic damage due to grain boundary cavities, the plastic damage as well as the creep damage is characterized by cavity distribution at grain boundaries. Then the damage states of the material may be expressed as a sum of the plastic damage tensor $\boldsymbol{\Omega}^P$ and the creep damage tensor $\boldsymbol{\Omega}^C$ as follows:

$$\boldsymbol{\Omega} = \boldsymbol{\Omega}^P + \boldsymbol{\Omega}^C, \tag{1}$$

where the *damage tensor* $\boldsymbol{\Omega}$ may be interpreted as an internal state variable which represents the three-dimensional area density of the grain boundary cavities[14]. Then

if we assume that the mechanical effects of this internal damage may be found in net area reduction due to cavity formation, the effects of the Cauchy stress $\boldsymbol{\sigma}$ are magnified to the corresponding *net stress tensor* $\mathbf{S}$ given by

$$\mathbf{S} = (\boldsymbol{\sigma}\boldsymbol{\Phi} + \boldsymbol{\Phi}\boldsymbol{\sigma})/2, \qquad \boldsymbol{\Phi} = (\mathbf{I} - \boldsymbol{\Omega})^{-1}, \tag{2}$$

where the tensor $\boldsymbol{\Phi}$ defines the magnification of the Cauchy stress $\boldsymbol{\sigma}$ as a result of material damage[14]; it will be called a *damage effect tensor* hereafter.

There may be two approaches to describe the evolution of the above damage tensor; one is to specify a damage surface in stress or strain space[9–12], while the other is to formulate directly the evolution equations of damage by taking account of the microscopic mechanisms of the cavity growth and their mechanical effects[8, 14, 29, 30]. As regards the former approach, in particular, Krajcinovic and Fonseka[11] introduced a damage surface $f = f(\boldsymbol{\epsilon}, \boldsymbol{\omega})$ in strain space by representing the damage state of brittle materials in terms of a cavity density vector $\boldsymbol{\omega}$; they formulated the evolution equations of damage by employing f as a potential surface of the damage rate. A similar notion was discussed also by Dragon and Mróz[10] by use of a second-rank crack density tensor $\boldsymbol{\Omega}$ proposed by Vakulenko and Kachanov[31] together with a damage surface $g(\boldsymbol{\sigma}, \boldsymbol{\Omega})$ or $h(\boldsymbol{\epsilon}, \boldsymbol{\Omega})$ in stress or strain space. In these theories, though the formulation of the evolution equation of damage variables is systematic and straightforward once the damage surfaces are specified properly, the determination of the shapes of the damage surfaces themselves and their variations need a number of damage tests and is considerably difficult. Regarding the plastic and creep damage mentioned above, on the other hand, the microscopic as well as the macroscopic features of the cavity growth have been elucidated sufficiently. Hence, in the following, we will take the second approach to formulate the evolution equations of the damage tensors $\boldsymbol{\Omega}^P$ and $\boldsymbol{\Omega}^C$ of eqn (1).

Let us first observe that both the damage tensors $\boldsymbol{\Omega}^P$ and $\boldsymbol{\Omega}^C$ represent the cavity area density produced by the grain boundary cavitations, and that the grain boundary cavitations are governed by the increase of the time-independent plastic strain $\boldsymbol{\epsilon}^P$ and the time t, respectively. If the effect of stress and damage on the rate of damage growth are expressed only through $\mathbf{S}$ and $\boldsymbol{\Phi}$ of eqn (2), the evolution equations of the plastic and creep damages may be given as

$$\mathrm{d}\boldsymbol{\Omega}^P = \mathbf{H}^P(\mathbf{S}, \boldsymbol{\Phi}, \boldsymbol{\epsilon}^P, \boldsymbol{\epsilon}^C)\,\mathrm{d}\boldsymbol{\epsilon}^P, \tag{3a}$$

$$\mathrm{d}\boldsymbol{\Omega}^C = \mathbf{H}^C(\mathbf{S}, \boldsymbol{\Phi}, \boldsymbol{\epsilon}^P, \boldsymbol{\epsilon}^C)\,\mathrm{d}t, \tag{3b}$$

where $\boldsymbol{\epsilon}^C$ denotes the creep strain tensor.

In particular, when the plastic deformation at room temperature develops under proportional loading, eqn (3a) can be integrated and leads to the form

$$\boldsymbol{\Omega}^P = \overline{\mathbf{H}}^P(\boldsymbol{\epsilon}^P). \tag{4}$$

Let us first recall that the tensor $\boldsymbol{\Omega}^P$ implies the area density of the grain boundary cavities induced in the damage process. Then if we further note the experimental results of Dyson *et al.*[6, 7] and observe that the cavities under proportional loading mainly develop on grain boundaries parallel to the principal stress direction (also, principal plastic strain direction), eqn (4) can be readily specified as

$$\boldsymbol{\Omega}^P = \gamma^P\mathbf{I} + \sum_{i=1}^{3} \mathbf{M}^{P(i)}[\boldsymbol{\nu}^{P(i)} \otimes \boldsymbol{\nu}^{P(i)}], \tag{5a}$$

where γ^P and $\mathbf{M}^{P(i)}$ are a scalar function and a fourth-rank tensor function of the plastic strain $\boldsymbol{\epsilon}^P$. The symbols $\boldsymbol{\nu}^{P(i)}$, $\mathbf{I}$ and $\otimes$ in eqn (5a), furthermore, denote the principal plastic strain direction of $\boldsymbol{\epsilon}^P$, the unit tensor and the tensor product, respectively.

The explicit form of the evolution eqn (3b), on the other hand, can be furnished

again from the experimental observations on creep damage process mentioned above[17, 22–25] and may be expressed in an analogous form[14]:

$$\dot{\Omega}^C = \gamma^C + \sum_{i=1}^{3} M^{C(i)}[\nu^{C(i)} \otimes \nu^{C(i)}] + \sum_{j=1}^{3} N^{C(j)}[\nu_D^{C(j)} \otimes \nu_D^{C(j)}], \tag{5b}$$

where γ^C, $M^{C(i)}$, $N^{C(j)}$ are a scalar function and fourth-rank tensor functions of S, Φ, ϵ^P and ϵ^C, respectively. The symbols $\nu^{C(i)}$ and $\nu_D^{C(j)}$ denote the principal directions corresponding to the positive principal values of S and its deviatoric tensor S_D.

Finally, if we assume that the effects of stress and damage on the creep of the damaged materials are expressed only through S and Φ of eqn (2), the constitutive equation of creep of the materials has the form

$$\dot{\epsilon}^C = G(S, \Phi, \epsilon^P, \epsilon^C). \tag{6}$$

3. CONSTITUTIVE AND EVOLUTION EQUATIONS OF CREEP DAMAGE

3.1. *Formulation of constitutive and evolution equations*

As observed from Fig. 1, creep of Nimonic 80A at 750°C under constant tension or constant torsion does not show any apparent primary creep stage but leads to the

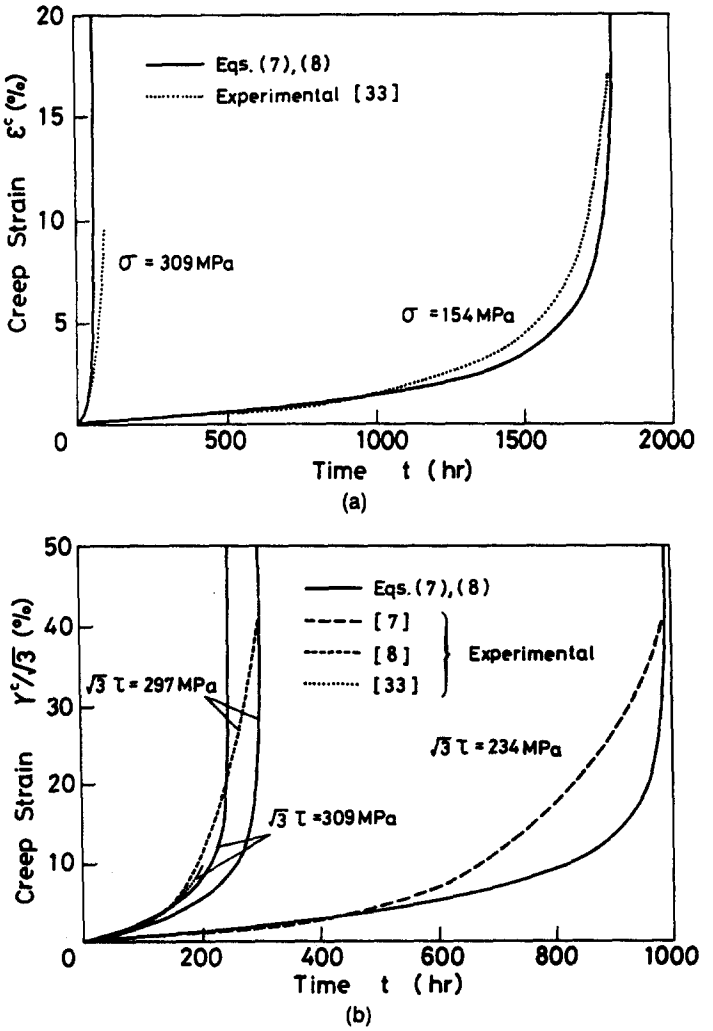

Fig. 1. Creep curves of Nimonic 80A at 750°C (unprestrained): (a) uniaxial tension; (b) torsion.

secondary stage from the beginning. If we assume that the creep rate in an undamaged state is governed by the flow rule and the equivalent stress of von Mises type and by Norton's law, the creep constitutive equation of damaged materials can be expressed in the form

$$\dot{\epsilon}^C = \tfrac{3}{2}A(S_{EQ})^{n-1}\,S_D, \tag{7a}$$

$$S_{EQ} = (\tfrac{3}{2}\mathrm{tr}\,S_D^2)^{1/2}, \tag{7b}$$

where S_{EQ} denotes the equivalent stress of S, and A and n are material constants.

Now, let us again note the metallurgical observations on the creep damage process reported so far[22–25, 32] and assume that the creep damage process is characterized by the formation of plane cavities on the grain boundary perpendicular to the maximum principal stress direction. Then eqn (5b) can be expressed in the more explicit form

$$\dot{\Omega}^C = B[\zeta S^{(1)} + (1-\zeta)S_{EQ}]^k[\mathrm{tr}(\Phi \nu^{C(1)} \otimes \nu^{C(1)})]^l(\nu^{C(1)} \otimes \nu^{C(1)}), \tag{8}$$

where $S^{(1)}$ and $\nu^{C(1)}$ denote the maximum principal stress and the corresponding direction of S; B, k, l and ζ are material constants.

According to the previous results of the creep damage tests on thin-walled copper tubes at 250°C[16], because of intrinsic anisotropy of creep cavity formation, the rotation of the principal stress direction prolongs the creep rupture times markedly in comparison with the creep rupture times under constant combined stress. The evolution equation (8) has been found to predict this trend adequately.

3.2. *Comparison between the theoretical and the experimental results on creep damage process*

Dotted or dashed curves of Figs. 1(a) and (b) show the results of tensile and torsional creep tests on thin-walled tubes of Nimonic 80A at 750°C. The creep curves for tensile stress $\sigma = 154$ and 309 MPa in Fig. 1(a) and that for torsional stress $\sqrt{3}\tau = 309$ MPa have been reproduced from Dyson and McLean's paper[33], while the creep curves for torsional stress $\sqrt{3}\tau = 234$ and 297 MPa in Fig. 1(b), respectively, are due to Dyson *et al.*[7] and Hayhurst *et al.*[8]. All the creep curves in Fig. 1 have been obtained on specimens of the identical size and subject to the identical heat treatment, and hence no significant scattering is observed among these curves.

Solid lines in Fig. 1, on the other hand, represent the theoretical curves fitted by eqns (7) and (8) to the corresponding experimental curves. Calculations of eqns (7) and (8) were performed by use of the following material constants:

$$\begin{aligned} A &= 9.14 \times 10^{-16}, \quad & n &= 4.56, \quad & \zeta &= 0.46, \\ B &= 1.732 \times 10^{-15}, \quad & k &= 5.0, \quad & l &= -2.3, \end{aligned} \tag{9}$$

where the units for stress and time are MPa and hr. The material constants of eqn (9) were determined in the following way.

Figure 2, to begin with, illustrates the relation between the equivalent stress $\bar{\sigma}$ and the equivalent minimum creep rate $\dot{\bar{\epsilon}}_m$ constructed from the creep rates of Fig. 1. The values of n and A of eqn (9) are determined from the slope and intercept of the straight line $\log \bar{\sigma} - \log \dot{\bar{\epsilon}}_m$ in this figure. Figure 3, furthermore, shows the relation between the creep rupture time t_R and the stress measure

$$\sigma^* = \alpha\sigma_1 + (1-\alpha)\bar{\sigma} \qquad (\alpha = 0.6) \tag{10}$$

obtained from Fig. 1, where σ_1 and α denote the maximum principal stress and a material constant. The constants k and B of eqn (9) were evaluated from the slope and the intercept of the straight line $\log \sigma^* - \log t_R$ of this figure. The value of ζ, furthermore, has been determined so that the rupture times for constant combined stress tests predicted by eqn (8) and the above values of B and k may be fit best to the corresponding

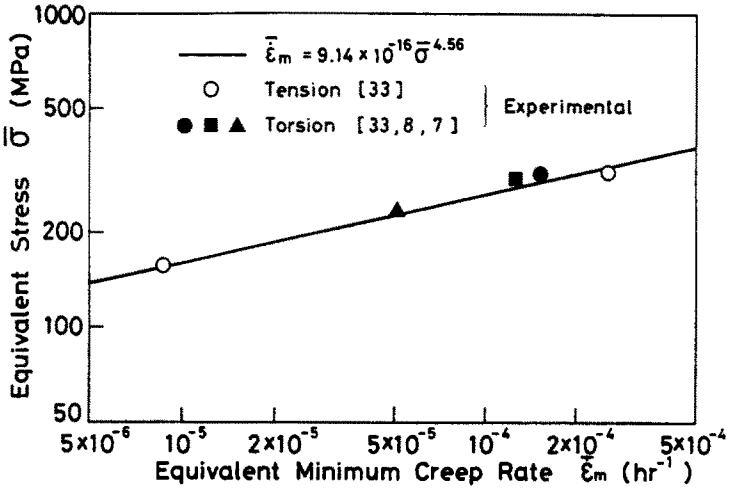

Fig. 2. Relation between equivalent stress and equivalent minimum creep rate.

experimental values. Finally, value of l was determined so that the tensile creep curves of Fig. 1(a) may be described most adequately by eqns (7)–(9).

As observed in Fig. 1(a), eqns (7) and (8) describe properly the creep curves of uniaxial tension as a whole. There is some discrepancy in the rupture times for σ = 309 MPa; it is because the material constants of eqn (9) have been determined with emphasis on the rupture times for σ = 154 MPa and those for torsional creep curves of Fig. 1(b).

Figure 1(b), on the other hand, shows that eqns (7) and (8) predict the rupture times of torsional creep tests accurately. However, as regards the creep behaviour, though eqns (7) and (8) can simulate the creep curves of the secondary stage, they give considerably smaller creep rates for the tertiary stages. This discrepancy can be accounted for partly by the stress state dependence of the cavity growth mode; i.e. the cavity density is smaller in torsion than in tension[7] (see Section 4.1). The mechanical effects of finite deformation and the effects of the third invariant of the deviatoric stress tensor on creep deformation may be also another source of the discrepancy.

Finally, in order to estimate the validity of eqns (7) and (8) applied to nonsteady states of stress, Fig. 4 compares the creep curves of the reversed torsion creep tests reported by Hayhurst *et al.*[8] with the corresponding predictions of eqns (7) and (8). Let us first compare the experimental curves of Fig. 4 with those of Fig. 1(b) of the

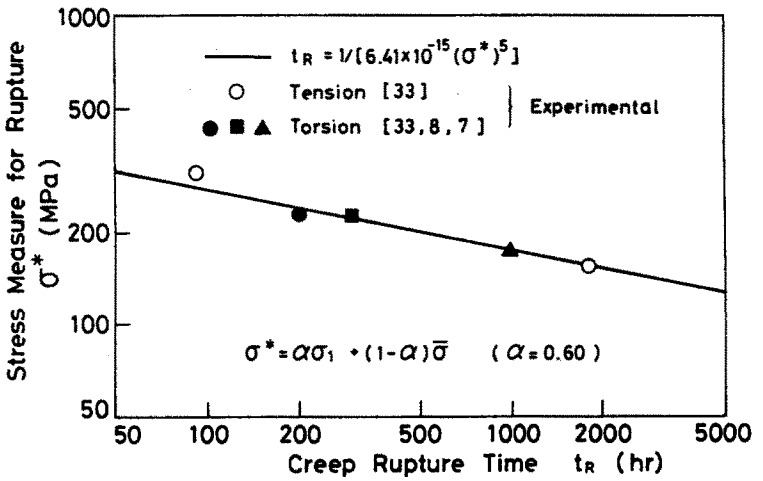

Fig. 3. Relation between creep rupture time and stress measure for rupture.

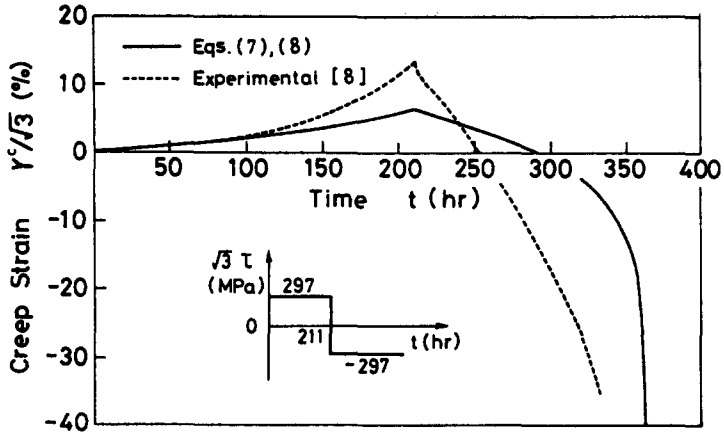

Fig. 4. Creep curves of Nimonic 80A at 750°C under reversed torsion (unprestrained).

same stress levels. The experimental creep rates of Fig. 4 up to the stress reversals coincide with those of Fig. 1(b) with accuracy better than 5%. Nevertheless, the creep rupture times for the constant and the reversed torsion test are t_R = 298 hr and 332 hr, respectively, and accordingly the reversed torsion test shows the rupture time about 11% longer than the constant torsion test. This result implies that the prolongation of the rupture time is attributable to the damage anisotropy (anisotropy of cavity formation) rather than the scattering of the experimental results.

The predicted rupture times of Fig. 1(b) and Fig. 4, on the other hand, are t_R = 300 hr and 363 hr and show the increase of rupture time observed in experiments. However, as seen in Fig. 4, eqns (7) and (8) give about 10% larger rupture time than the experiment, and this feature can be accounted for by the simplified assumption on the cavity growth mode in eqn (8), besides the scattering in experimental results.

4. FORMULATION OF EVOLUTION EQUATION OF PLASTIC DAMAGE

4.1. *Experimental observations on plastic damage*

Dyson and Rodgers[6] performed tensile creep tests at 750°C on Nimonic 80A specimens subjected to prior tension at room temperature, and made metallographical observations on crept specimens by means of an optical microscope. As a result of these tests, a number of grain boundary cavities were observed in the crept and the fractured specimens, and the number of these cavities increased with the increasing magnitude of prestrains. It was also elucidated that these cavities brought about salient deleterious effects on creep properties, i.e. decrease in creep strength, creep rupture time and creep ductility (see Figs 6 and 7).

In order to explicate the plastic damage under various states of stress, Dyson, Loveday and Rodgers[7] further made a series of quantitative observations by means of a 1-MV electron microscope on Nimonic 80A specimens, subjected to prior plastic strains under tension, compression and torsion and then annealed for two hours at 750°C. They found that, though profuse submicrometer grain boundary cavities were produced by any of these three stress states and the numbers of cavities per unit volume were functions of the effective prior plastic strain, the cavity density for a given effective plastic strain was the largest for tension prestrain and decreased in the order of torsion and compression. Then it was also revealed that most of these cavities were formed on those grain boundaries parallel to the maximum principal stress direction and, hence, had pronounced anisotropy. This anisotropy in cavity formation, furthermore, was more salient for torsional prestrain than tensile and compressive ones. Because of such anisotropy of plastic damage, forward pretorsion and reverse pretorsion have significantly different effects on the subsequent torsional creep (see Fig. 7).

4.2. *Representation of plastic damage state in Nimonic 80A and its specialization*

As mentioned above, plastic deformations at room temperature have various effects on the subsequent creep properties of Nimonic 80A. For accurate description of creep in such prestrained materials, it is necessary first to quantify appropriately the internal states of damage induced by the plastic deformation.

Let us now assume that the states of plastic damage can be described by a second-rank symmetric damage tensor Ω^P of eqn (5a). From the viewpoint of continuum damage mechanics, this damage variable is interpreted as a macroscopic internal state variable averaged over a small element in the material; its mechanical effect on macroscopic phenomena is usually identified only through macroscopic physical quantities, and it is not straightforward to correlate the damage variable with the results of the micrographical observations reported by Dyson *et al.*[7, 33]. Thus, we will now evaluate the variable Ω^P from the creep rupture times in the subsequent creep tests observed in Figs 6 and 7.

If we recall the assumption of eqn (1), the creep damage equation (8) in uniaxial state with tensile plastic prestrain has the form

$$\dot{\Omega}^C = B[\sigma^k/(1 - \Omega)^{k+l}] = B[\sigma^k/(1 - \Omega^C - \Omega^P)^{k+l}]. \tag{11}$$

Integrating eqn (11) with the initial condition $\Omega^C = 0$ at $t = 0$, and taking account of the rupture condition $\Omega = \Omega^C + \Omega^P = 1$ at $t = t_R$, we readily obtain the creep rupture time $(t_R)_{\epsilon^P}$ of prestrained materials as follows:

$$(t_R)_{\epsilon^P} = (1 - \Omega^P)^{k+l+1}/[B(k + l + 1)\sigma^k]. \tag{12}$$

The creep rupture time $(t_R)_0$ of unprestrained materials, in particular, can be furnished from eqn (12) by taking $\Omega^P = 0$:

$$(t_R)_0 = 1/[B(k + l + 1)\sigma^k]. \tag{13}$$

Thus, eqns (12) and (13) enable us to specify the plastic damage Ω^P in the following form:

$$\Omega^P = 1 - [(t_R)_{\epsilon^P}/(t_R)_0]^{1/(k+l+1)}. \tag{14}$$

A similar relation is obtained also for the creep rupture tests under torsion after torsional prestrain, and eventually we have the following relation for simple states of stress:

$$\Omega^P = 1 - [(t_R)_{\bar{\epsilon}^P}/(t_R)_0]^{1/(k+l+1)}, \tag{15}$$

where $(t_R)_{\bar{\epsilon}^P}$ denotes the creep rupture time under equivalent plastic prestrain $\bar{\epsilon}^P$.

Figure 5 illustrates the relation between plastic damage Ω^P and equivalent plastic prestrain $\bar{\epsilon}^P$ calculated from eqn (15) and the experimental results of the literature entered in the figure. Namely, the symbol ○ in the figure represents the results of tensile creep tests following tensile plastic prestrains[6], while the symbols △, ◨, ▲ and ■ are those of torsion creep tests after torsional prestrains[7, 8] shown in Fig. 7.

As observed in this figure, the plastic damage Ω^P increases with the increase of the equivalent plastic prestrain $\bar{\epsilon}^P$ in any cases of tension and torsion. In the case of tensile prestrain, in particular, the $\log \Omega^P - \log \bar{\epsilon}^P$ relation can be represented by a straight line. However, for a given value of equivalent plastic prestrains, the plastic damage for torsional prestrain (symbols △, ◨, ▲ and ■) are somewhat smaller than those for tensile prestrain (symbol ○). This trend coincides with the metallographical observations of Dyson *et al.*[7] mentioned above, which revealed that the number of grain boundary cavities produced by tensile prestrain was larger than that produced by torsional prestrain. From a continuum mechanics point of view this trend can be

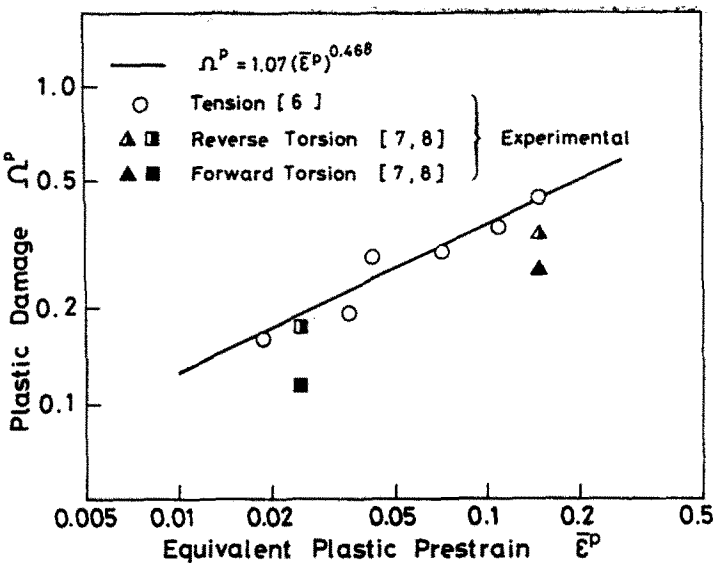

Fig. 5. Relation between plastic damage and equivalent plastic prestrain at room temperature.

expressed as the dependence of plastic damage on the second and the third invariants of the deviatoric plastic strain tensor defined as follows:

$$K_2 = \tfrac{1}{2}\epsilon^P_{ij}\epsilon^P_{ij}, \qquad K_3 = \tfrac{1}{3}\epsilon^P_{ij}\epsilon^P_{jk}\epsilon^P_{ki}. \tag{16}$$

The second characteristic observed in Fig. 5 is the significant difference between plastic damage Ω^P due to reverse plastic pretorsion (▲, ◨) and that of forward plastic pretorsion (▲, ■). This can be accounted for by a significant influence of the interaction between anisotropies of plastic and creep damages on creep rupture times. As mentioned already, submicrometer cavities due to plastic damage are formed mostly on grain boundaries parallel to the maximum principal stress direction. In view of this oriented nature of cavity arrangement together with the above-mentioned trend, eqn (5a) can be specialized in the following form:

$$\begin{aligned}\boldsymbol{\Omega}^P &= f(K_2, K_3)[\boldsymbol{\nu}^{P(2)} \otimes \boldsymbol{\nu}^{P(2)} + \boldsymbol{\nu}^{P(3)} \otimes \boldsymbol{\nu}^{P(3)}] + g(K_2, K_3)\mathbf{I} \\ &= f(K_2, K_3)[\mathbf{I} - \boldsymbol{\nu}^{P(1)} \otimes \boldsymbol{\nu}^{P(1)}] + g(K_2, K_3)\mathbf{I}.\end{aligned} \tag{17}$$

The first term on the right-hand side of this equation represents the anisotropic effect of the grain boundary cavities, while the second term describes the isotropic feature of the plastic damage.

As simple and explicit forms of the functions f and g of eqn (17), we can take

$$f(K_2, K_3) = F[\tfrac{1}{3}K_2]^{\mu/2}, \qquad g(K_2, K_3) = G[4K_3]^{\nu/3}, \tag{18}$$

where F, G, μ and ν are material constants. For torsional plastic prestrain, eqn (18) gives $g(K_2, K_3) = 0$, and hence eqn (17) provides the largest anisotropy. For tensile prestrain, on the other hand, we have $g(K_2, K_3) \neq 0$, and eqn (17) describes the isotropic damage growth as well. Thus, for a given value of equivalent plastic prestrain, the cavity volume fraction tr $\boldsymbol{\Omega}^P$ for tensile prestrain has a larger value than that for torsional prestrain, so that eqns (17) and (18) describe adequately the characteristic features observed in the paper of Dyson *et al.*[7].

The material constants in eqns (17) and (19) were specified as

$$F = 0.806, \quad \mu = 0.323, \quad G = 1.07, \quad \nu = 0.468. \tag{19}$$

The values of G and ν among them were obtained from the slope and the intercept of the $\log \Omega^P - \log \bar{\epsilon}^P$ relation (Fig. 5) for tensile plastic prestrain. The values of F and μ, on the other hand, were specified so that eqns (15), (17) and (18) may describe the rupture times for torsional creep subjected to reverse plastic prestorsion.

Finally, we assume that the creep constitutive equation (7) and the evolution equation of creep damage (8) hold also for the plastically damaged materials:

$$\dot{\epsilon}^C = \tfrac{3}{2}A(S_{EQ})^{n-1}\mathbf{S}_D, \tag{20a}$$

$$\dot{\Omega}^C = B[\zeta S^{(1)} + (1 - \zeta)S_{EQ}]^k[\mathrm{tr}(\Phi \boldsymbol{\nu}^{C(1)} \otimes \boldsymbol{\nu}^{C(1)})]^l (\boldsymbol{\nu}^{C(1)} \otimes \boldsymbol{\nu}^{C(1)}). \tag{20b}$$

In these equations the effects of plastic damage can be described by means of the relation (1) together with the net stress tensor $\mathbf{S}$ and the damage effect tensor Φ defined by eqn (2). Furthermore, the material constants of eqn (20) are furnished by eqn (9).

5. RESULTS OF CALCULATIONS AND COMPARISON WITH EXPERIMENTAL RESULTS

We are now in a position to analyse the creep damage process of Nimonic 80A at 750°C subjected to plastic prestrains of tension and torsion at room temperature by means of the above equations.

Figure 6, to begin with, compares the result of tensile creep tests subjected to tensile prestrain of $\epsilon^P = 15\%$ with the corresponding prediction of eqns (17)–(20). The dashed line is the experimental curve obtained by Hayhurst *et al.*[8], whereas the solid line is the theoretical curve. In Fig. 6, tensile creep curves of unprestrained (virgin) materials and the corresponding numerical result are also entered for the sake of comparison. For unprestrained materials, in particular, the scale of abscissa has been magnified to 10 times.

As will be seen in the figure, creep property of the prestrained material differs largely from that of the unprestrained material. For example, the experimental results for the minimum creep rate $\dot{\epsilon}_m$ of the unprestrained and the prestrained material are $\dot{\epsilon}_m = 9 \times 10^{-6}\ \mathrm{hr}^{-1}$, $8 \times 10^{-5}\ \mathrm{hr}^{-1}$, respectively, and thus the plastic prestrain of $\epsilon^P = 15\%$ magnified the creep rate almost by 10 times. Furthermore, the creep strains at rupture for the unprestrained and the prestrained material are $\epsilon_R = 18\%$ and 2.7%, respectively, while the corresponding creep rupture times are $t_R = 1800$ hr and 206 hr. Thus, it will be found that the plastic prestrain markedly curtails the creep ductility

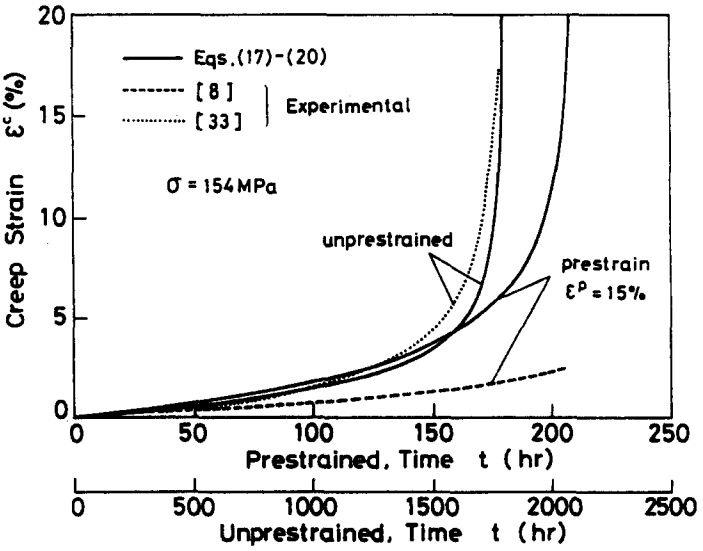

Fig. 6. Tension creep curves after plastic pretension at room temperature (Nimonic 80A, 750°C).

and the creep rupture time. Similar trends are observed also for different magnitudes of plastic prestrain[6].

Equations (17)–(20), on the other hand, describe properly the increase of minimum creep rates and the decrease of rupture times due to plastic prestrains, as discussed above. However, these equations tend to give larger creep rates than the experimental ones in later parts of creep curves and, accordingly, predict larger creep strains at rupture. Though these discrepancies can be partly accounted for by the possible scattering of the experimental results, they are also attributable to salient localization of the cavity distribution observed in prestrained materials, which has not been incorporated in the present theory. Namely, according to the optical micrography mentioned already[6], in highly prestrained specimens, a number of crack-like cavities produced by coalesced r-type cavities were observed in many areas near the fractured surface, and the cavity densities in these areas were apparently larger than other parts. Such a localized creep damage induced by larger plastic prestrains may shorten the tertiary creep stages of prestrained materials and may decrease the creep ductility of these materials. Therefore, in order to describe the experimental results of Fig. 6 more accurately by the present theory, we must further elaborate eqns (17)–(20) to represent the difference in damage localization in the unprestrained and prestrained materials.

Figures 7(a) and (b), furthermore, compares similar results for torsional creep curves of materials subjected to different plastic pretorsions. The dashed curves in the figures represent the experimental results of Dyson *et al.*[7] and Hayhurst *et al.*[8],

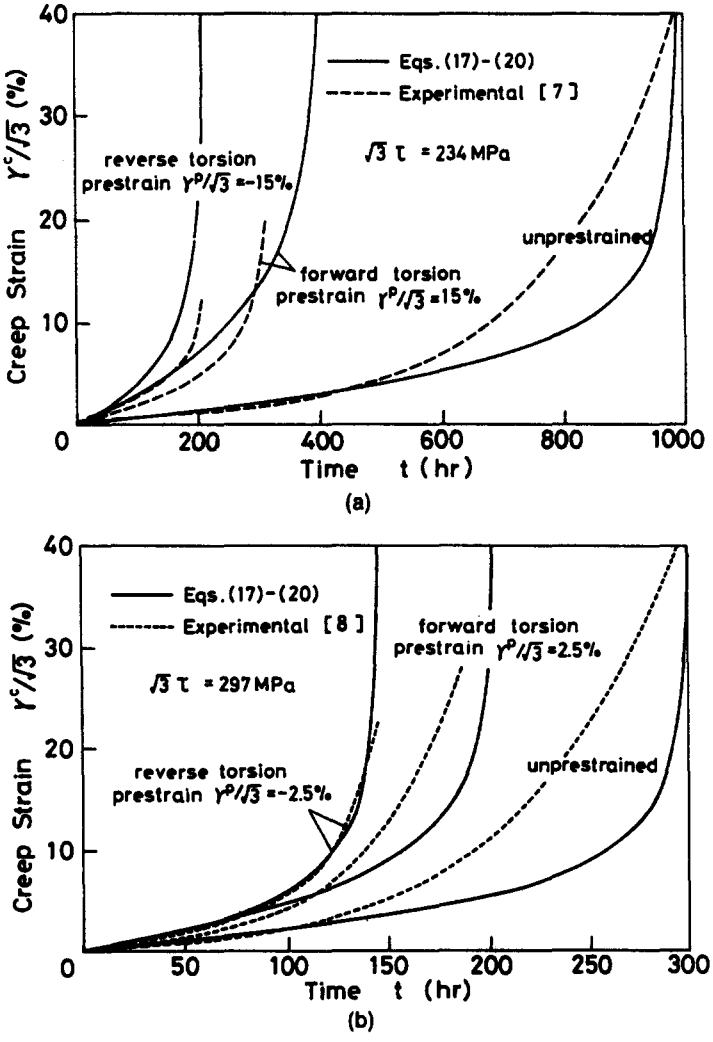

Fig. 7. Torsion creep curves after plastic pretorsion at room temperature (Nimonic 80A, 750°C): (a) $\sqrt{3}\tau$ = 234 MPa; (b) $\sqrt{3}\tau$ = 297 MPa.

while the solid curves are the theoretical predictions due to eqns (17)–(20). The corresponding results for the unprestrained material are also entered in the figure.

One of the remarkable features observed in Figs. 7(a) and (b) is a salient dependence of torsional creep process on the direction of prior plastic torsion. For example, the experimental results of creep rupture time t_R for the forward and the reverse pretorsion, respectively, are t_R = 311 hr and 207 hr for $\sqrt{3}\tau$ = 234 MPa and $\bar{\epsilon}^P$ = 15% [Fig. 7(a)], and t_R = 188 hr and 146 hr for $\sqrt{3}\tau$ = 297 MPa and $\bar{\epsilon}^P$ = 2.5% [Fig. 7(b)]. These differences in rupture times obviously result from the anisotropy in the plastic and the creep damages and can be explained as follows. As mentioned already, while grain boundary cavities due to plastic damage are produced mainly on grain boundaries parallel to the maximum principal stress direction, creep cavities develop mostly on grain boundaries perpendicular to the maximum principal stress direction. In materials subjected to forward plastic pretorsion, for example, since the principal stress direction corresponding to the plastic pretorsion coincides with that for the subsequent torsional creep, the creep cavities develop on separate planes, which are different from the planes of significant plastic cavities and are rotated by 90° from them. In the case of reverse plastic pretorsion, on the other hand, the principal stress direction for the plastic pretorsion differs by 90° from that of the torsional creep, and therefore the creep cavities develop predominantly on the same plane where the preceding plastic cavities have been produced. Thus, the creep damage process subjected to reverse plastic pretorsion is accelerated considerably, and the corresponding rupture time is shorter than that of the forward pretorsion. This marked dependence of the creep damage process on the direction of prior plastic strain can never be described by isotropic damage theories developed so far.

On the other hand, the creep rupture times t_R calculated from eqns (17)–(20) for the forward and the reverse pretorsions are t_R = 402 hr and 207 hr, respectively, in the case of $\sqrt{3}\tau$ = 234 MPa, $\bar{\epsilon}^P$ = 15% [Fig. 7(a)], and t_R = 202 hr and 145 hr for $\sqrt{3}\tau$ = 297 MPa, $\bar{\epsilon}^P$ = 2.5% [Fig. 7(b)]. Thus, the present theory predicts properly the trend of experimental results. However, detailed observation of Fig. 7 shows that eqns (17)–(20) give the rupture times for forward plastic pretorsion 10–20% larger than the experiment. These discrepancies can be accounted for by the simplified assumption in eqn (20) concerning the planes of damage growth, as well as by the assumption of a simple form of g in eqn (18). Nevertheless, it should be noted that the discrepancies between theoretical and experimental results of rupture times observed in Fig. 7 are rather insignificant from a practical point of view.

In contrast to the discrepancies between the theoretical and experimental creep curves for unprestrained materials, it will be noticed that eqns (17)–(20) describe apparently well the creep curves of prestrained materials as a whole. This trend can be explained as the counterbalance between the smaller creep rates in the tertiary stage of unprestrained materials predicted by eqns (17)–(20) and the enhanced creep rates observed in the prestrained materials due to damage localization. However, these two separate effects result from the complicated dependence of cavity arrangement (size, shape, density, anisotropy, nonhomogeneity) on the stress level or the stress state.

The present problem has been analyzed also by Hayhurst, Trampczynski and Leckie[8]. They modified the quasi-empirical metallurgical theory of Dyson and McLean[33] by incorporating the effect of grain boundary cavities due to the plastic prestrain into the evolution equation of the total cavity volume fraction for the subsequent creep damage process, and they succeeded in providing reasonable predictions to the creep rates and the creep rupture times of the prestrained materials [i.e. to experimental curves of Figs 6 and 7(b)]. However, their theory postulated isotropic damage parameter of the cavity volume fraction and could not describe the anisotropic aspects of the material damage observed in the forward and the reversed creep curves of Fig. 7(b).

6. CONCLUSIONS

After formulating the coupled phenomena of the plastic and the creep damages of polycrystalline metals, the effects of the plastic damage induced by various plastic

prestrains at room temperature on the subsequent creep damage process of Nimonic 80A at 750°C were analysed. The proposed theory not only described adequately the pronounced decrease in creep strength and creep rupture time, but also represented anisotropic features in these damages. However, it was found that more accurate simulation of the creep behaviour of the damaged materials will need further elaborate modelling of damage and creep.†

Acknowledgement—The authors are grateful to Associate Professor N. Ohno of Toyohashi University of Technology for his valuable comments and discussion on this paper.

REFERENCES

1. J. Hult, CDM—capabilities, limitations and promises. In *Mechanisms of Deformation and Fracture* (Edited by K. E. Easterling), pp. 233–247. Pergamon Press, Oxford (1979).
2. J. Lemaitre and J. L. Chaboche, Aspect phénoménologique de la rupture par edommagement. *J. Méc. Appl.* **2**, 317–365 (1978).
3. J. Lemaitre, Damage modelling for prediction of plastic or creep fatigue failure in structures. In *Trans. 5th Int. Conf. on Structural Mechanics in Reactor Technology* (Edited by T. A. Jaeger and B. A. Boley), paper no. L5/1*b. North-Holland, Amsterdam (1979).
4. J. L. Chaboche, Continuous damage mechanics—a tool to describe phenomena before crack initiation. *Nucl. Engng Design* **64**, 233–247 (1981).
5. S. Murakami, Anisotropic damage in metals. In *Failure Criteria of Structured Media* (Edited by J. P. Boehler). Balkema, Rotterdam (1986).
6. B. F. Dyson and M. J. Rodgers, Prestrain, cavitation, and creep ductility. *Metal Sci.* **8**, 261–266 (1974).
7. B. F. Dyson, M. S. Loveday and M. J. Rodgers, Grain boundary cavitation under various states of applied stress. *Proc. Roy. Soc. London A* No. 349, 245–259 (1976)).
8. D. R. Hayhurst, W. A. Trampczynski and F. A. Leckie, Creep-rupture under non-proportional loading. *Acta Metall.* **28**, 1171–1183 (1980).
9. J. W. Dougil, On stable progressively fracturing solids. *J. Appl. Math. Phys. (ZAMP)* **27**, 423–437 (1976).
10. A. Dragon and Z. Mróz, A continuum model for plastic–brittle behaviour of rock and concrete. *Int. J. Engng Sci.* **17**, 121–137 (1979).
11. D. Krajcinovic and G. U. Fonseka, The continuum damage theory of brittle materials. Part 1: General theory. *ASME J. Appl. Mech.* **48**, 809–815 (1981).
12. J. P. Cordebois and F. Sidoroff, Endommagement anisotrope en élasticité et plasticité. *J. Méc. Théor. Appl.* Numéro Spécial, 45–60 (1982).
13. S. Murakami, Notion of continuum damage mechanics and its application to anisotropic creep damage theory. *ASME J. Engng Mat. Tech.* **105**, 99–105 (1983).
14. S. Murakami and N. Ohno, A continuum theory of creep and creep damage. In *Creep in Structures* (Edited by A. R. S. Ponter and D. R. Hayhurst), pp. 422–444. Springer, Berlin (1981).
15. S. Murakami and T. Imaizumi, Mechanical description of creep damage state and its experimental verification. *J. Méc. Théor. Appl.* **1**, 743–761 (1982).
16. S. Murakami and Y. Sanomura, Creep and creep damage of copper under multiaxial states of stress. In *Plasticity Today* (Edited by A. Sawczuk and G. Bianchi), pp. 535–551. Elsevier Applied Science, London (1985).
17. A. S. Tetelman and A. J. McEvily, Jr., *Fracture of Structural Materials*. John Wiley, New York (1968).
18. J. F. Knott, *Fundamentals of Fracture Mechanics*. Butterworth, London (1977).
19. M. F. Ashby, C. Gandhi and D. M. R. Taplin, Fracture-mechanism maps and their construction for f. c. c. metals and alloys. *Acta Metall.* **27**, 699–729 (1979).
20. C. Gandhi and M. F. Ashby, Fracture-mechanism maps for materials which cleave: f. c. c., b. c. c. and h. c. p. metals and ceramics. *Acta Metall.* **27**, 1565–1602 (1979).
21. S. H. Goods and L. M. Brown, The nucleation of cavity by plastic deformation. *Acta Metall.* **27**, 1–15 (1979).
22. M. F. Ashby and R. Raj, Creep fracture. In *The Mechanics and Physics of Fracture*, Metals Society and Institute of Physics, pp. 148–158. The Metal Society, London (1975).
23. R. Lagneborg, Creep: mechanisms and theories. In *Creep and Fatigue in High Temperature Alloys* (Edited by J. Bressers), pp. 41–71. Elsevier Applied Science, London (1981).
24. F. Garofalo, *Fundamentals of Creep and Creep-Rupture in Metals*. Macmillan, New York (1965).
25. A. S. Argon, Mechanisms and mechanics of fracture in creeping alloys. In *Recent Advances in Creep and Fracture of Engineering Materials and Structures* (Edited by B. Wilshire and D. R. J. Owen), pp. 1–52. Pineridge, Swansea (1982).
26. H. Broberg, A new criterion for brittle creep rupture. *ASME J. Appl. Mech.* **41**, 809–811 (1974).
27. J. Hult, Creep in continua and structures. In *Topics in Applied Continuum Mechanics* (Edited by J. L. Zeman and F. Ziegler), pp. 137–155. Springer, Vienna (1974).
28. L. M. Kachanov, *Foundations of Fracture Mechanics*. Izdat. Nauka, Moscow (1974) (in Russian).
29. L. Davison and A. L. Stevens, Thermodynamical constitution of spalling elastic bodies. *J. Appl. Phys.* **44**, 668–674 (1973).

† More accurate analysis of this problem by taking account of the finite deformation and a new constitutive equation of creep will be discussed in Ref. [35].

30. J. L. Chaboche, Le concept de contrainte effective appliqué à l'élasticité et à la viscoplasticité en présence d'un endommagement anisotrope. In *Mechanical Behavior of Anisotropic Solids* (Edited by J. P. Boehler), pp. 737–760. Martinus Nijhoff, The Hague (1982).
31. A. A. Vakulenko and M. L. Kachanov, Continuum theory of cracked media. *Mech. Tverdogo Tiela* No. 4, 159–166 (1971) (in Russian).
32. D. R. Hayhurst, Creep rupture under multi-axial states of stress. *J. Mech. Phys. Solids* **20**, 381–390 (1972).
33. B. F. Dyson and D. McLean, Creep of Nimonic 80A in torsion and tension. *Metal Sci.* **11**, 37–45 (1977).
34. H. E. Evans, *Mechanisms of Creep Fracture*. Elsevier Applied Science, London (1984).
35. S. Murakami and Y. Sanomura, Analysis of the coupled effect of plastic damage and creep damage in Nimonic 80A at finite deformation. *Engng Fracture Mech.* (1986), in press.